Monthly Notices of the ROYAL ASTRONOMICAL SOCIETY

MNRAS **545,** 1–14 (2026) https://doi.org/10.1093/mnras/staf2143
Advance Access publication 2025 December 04

Cosmological constraints from galaxy clustering and galaxy–galaxy lensing with extended SubHalo Abundance Matching

Constance Mahony [1,2★], Sergio Contreras [1,3], Raul E. Angulo [1,4], David Alonso,[2] Christos Georgiou [5,6] and Andrej Dvornik[7]

[1]*Donostia International Physics Center, Manuel Lardizabal Ibilbidea, 4, E-20018 Donostia, Gipuzkoa, Spain*
[2]*Department of Physics, University of Oxford, Denys Wilkinson Building, Keble Road, Oxford OX1 3RH, UK*
[3]*Facultad de Física, Universidad de Sevilla, Multidisciplinary Unit for Energy Science, Av. Reina Mercedes s/n, E-41012 Seville, Spain*
[4]*IKERBASQUE, Basque Foundation for Science, E-48013 Bilbao, Spain*
[5]*Institute for Theoretical Physics, Utrecht University, Princetonplein 5, NL-3584 CC Utrecht, the Netherlands*
[6]*Institut de Física d'Altes Energies (IFAE), The Barcelona Institute of Science and Technology, Campus UAB, E-08193 Bellaterra (Barcelona), Spain*
[7]*Faculty of Physics and Astronomy, Ruhr University Bochum, Astronomical Institute (AIRUB), German Centre for Cosmological Lensing, D-44780 Bochum, Germany*

Accepted 2025 December 1. Received 2025 November 27; in original form 2025 July 2

ABSTRACT

We present the first cosmological constraints from a joint analysis of galaxy clustering and galaxy–galaxy lensing using extended SubHalo Abundance Matching (SHAMe). We analyse stellar mass-selected Galaxy And Mass Assembly galaxy clustering and Kilo-Degree Survey (KiDS-1000) galaxy–galaxy lensing and find constraints on $S_8 \equiv \sigma_8\sqrt{\Omega_{\rm m}/0.3} = 0.793^{+0.025}_{-0.024}$, in agreement with *Planck* at 1.7σ, with σ_8 the mass density fluctuation amplitude in 8 h^{-1}Mpc sphere at present and $\Omega_{\rm m}$ the density parameter in total matter. These results are in agreement with the cosmic microwave background results from *Planck*. We are able to constrain all five SHAMe parameters, which describe the galaxy–subhalo connection. We validate our methodology by first applying it to simulated catalogues, generated from the TNG300 simulation, which mimic the stellar mass selection of our real data. We show that we are able to recover the input cosmology for both our fiducial and all-scale analyses. Our all-scale analysis extends to scales of galaxy–galaxy lensing below $r_{\rm p} < 1.4\,{\rm Mpc}\,h^{-1}$, which we exclude in our fiducial analysis to avoid baryonic effects. When including all scales, we find a value of S_8, which is 1.26σ higher than our fiducial result (against naive expectations where baryonic feedback should lead to small-scale power suppression), and in agreement with *Planck* at 0.9σ. We also find a 21 per cent tighter constraint on S_8 and a 29 per cent tighter constraint on $\Omega_{\rm m}$ compared to our fiducial analysis. This work shows the power and potential of joint small-scale galaxy clustering and galaxy–galaxy lensing analyses using SHAMe.

Key words: cosmological parameters – large-scale structure of the Universe.

1 INTRODUCTION

Imaging galaxy surveys have been highly successful at constraining the current cosmological model (C. Heymans et al. 2021; T. M. C. Abbott et al. 2022; H. Miyatake et al. 2023). In particular, they have placed constraints on the matter density of the Universe $\Omega_{\rm m}$ and the amplitude of matter fluctuations[1] S_8 that are now competitive with cosmic microwave background (CMB) experiments (Planck Collaboration VI 2020). The most powerful results generally come from combining measurements of the clustering of galaxies, how dark matter mildly distorts galaxy images via weak gravitational lensing, and how the structure traced by foreground galaxies distorts background galaxy images (galaxy–galaxy lensing). Recently, there has been much discussion regarding a potential tension between the value of S_8 recovered by galaxy surveys and that preferred by CMB data within the Lambda cold dark matter (ΛCDM) model, with one of the main proposed solutions being potential uncertainties in the modelling of these three observables on small scales (M. Yoon et al. 2019; M. Yoon & M. J. Jee 2021; A. Amon & G. Efstathiou 2022; G. Aricò et al. 2023; C. Preston, A. Amon & G. Efstathiou 2023; C. García-García et al. 2024). While recent weak lensing results from the Kilo-Degree Survey (KiDS) show no tension with the CMB (B. Stölzner et al. 2025; A. H. Wright et al. 2025), ensuring accurate modelling of all observables on small scales remains a priority.

A common conservative approach to mitigating small-scale uncertainties is to apply scale cuts to the data, removing data points where these biases are most likely to be relevant (e.g. E. Krause et al. 2021). However, there are two problems with this. One is that this approach involves discarding a huge amount of data, which have a wealth of information about galaxies as well as cosmology. The

★ E-mail: constance.mahony@physics.ox.ac.uk

[1]As is usual, we will quantify the amplitude of matter fluctuations in terms of σ_8: the standard deviation of the linear matter overdensity field on spheres of 8 h^{-1} Mpc radius, where h is the Hubble constant in units of 100 km s^{-1} Mpc^{-1}. We will also use the 'clumping' parameter S_8, defined in terms of σ_8 and $\Omega_{\rm m}$ as $S_8 \equiv \sigma_8\,(\Omega_m/0.3)^{0.5}$.

second is that it is difficult to cleanly remove uncertain non-linear and astrophysical processes that are not fully localized in either Fourier or configuration space from common observables. Both of these issues will be more acute for the next generation of surveys, such as *Euclid* (Euclid Collaboration 2025) and the Vera C. Rubin Observatory Legacy Survey of Space and Time (LSST; Ž. Ivezić et al. 2019), which are already underway.

The difficulty in modelling small scales comes from linking the properties and spatial distribution of galaxies to the underlying matter inhomogeneities. On large scales, this relationship is linear and simple to model. However, on small scales, the relationship is non-linear, non-local, and non-deterministic. One approach to is to expand the bias perturbatively, which has been shown to be very successful at extending analyses to intermediate scales (e.g. F. Beutler et al. 2017; M. M. Ivanov, M. Simonović & M. Zaldarriaga 2020; G. d'Amico et al. 2020; A. Nicola et al. 2024). To extend analyses to even smaller scales, while achieving the necessary accuracy, requires detailed modelling of the astrophysics of galaxies. Usually, this modelling is divided into two parts: how matter clusters into dark matter haloes and how galaxies populate these haloes. The distribution of dark matter haloes is either calculated analytically through the halo model (R. E. Smith et al. 2003; R. Takahashi et al. 2012; A. J. Mead et al. 2021), taken directly from dark matter simulations (T. Nishimichi et al. 2019; H. Miyatake et al. 2022) or a combination of the two (A. J. Mead & L. Verde 2021; C. Mahony et al. 2022). Then these dark matter haloes are populated with galaxies in a second step.

There are two main approaches to populating dark matter haloes with galaxies. The first more popular approach is Halo Occupation Distribution (HOD) modelling, which provides a probabilistic description for this process. This approach is successful in predicting galaxy distributions (e.g. S. Contreras et al. 2024), but it requires a large number of parameters and typically does not account for variable levels of assembly bias. Assembly bias refers to how the evolutionary history of haloes impacts the clustering of their associated galaxies, not only their mass (L. Gao, V. Springel & S. D. M. White 2005; R. H. Wechsler et al. 2006; N. Dalal et al. 2008). Some extensions to HOD modelling do include assembly bias (A. P. Hearin et al. 2016), but these approaches further increase the parameter space. The second approach is SubHalo Abundance Matching (SHAM), which matches a dark matter subhalo property to a corresponding galaxy property. Usually, SHAM relates a property summarizing the mass of a dark matter subhalo to the stellar mass or luminosity of a galaxy. Here, the assumption is that more massive subhaloes tend to host more luminous galaxies. SHAM can reproduce both real observations of galaxies (S. Contreras, J. Chaves-Montero & R. E. Angulo 2023c) and results from hydrodynamic simulations (J. Chaves-Montero et al. 2016; S. Contreras et al. 2023a). The main advantages of SHAM over HOD approaches is that SHAM utilizes fewer parameters and includes a variable level of assembly bias. The main disadvantage is that SHAM requires subhalo information, which is computationally expensive and is a key factor in why SHAM has not previously been used for cosmological analyses of galaxy clustering and galaxy–galaxy lensing. However, it is possible to overcome these challenges by emulating the observables, and access to subhalo information aids in modelling the distribution of satellite galaxies, which is particularly useful for galaxy–galaxy lensing (J. Chaves-Montero, R. E. Angulo & S. Contreras 2023; S. Contreras et al. 2023a).

Previous works have used HOD modelling to place tight constraints on S_8 and Ω_m from combined analyses of small-scale galaxy clustering and galaxy–galaxy lensing (A. Dvornik et al. 2023; H. Miyatake et al. 2023). In this work, we obtain the first cosmological constraints from a combined analysis of galaxy clustering and galaxy–galaxy lensing using the SHAM method. In Section 2, we present our extended SHAM methodology, and detail the creation of our galaxy clustering and galaxy–galaxy lensing emulator. In Section 3, we present the galaxy clustering and galaxy–galaxy lensing data used in the analysis. In Section 4, we validate our methodology on a simulated galaxy sample before presenting our results for real data in Section 5. We conclude in Section 6.

2 METHODOLOGY

2.1 Extended abundance matching

In most implementations, the SHAM model has one free parameter, the scatter between a given subhalo property (e.g. mass or circular velocity) and the related galaxy property used to rank them (e.g. stellar mass or luminosity). However, these implementations provide limited precision and S. Contreras, R. E. Angulo & M. Zennaro (2021c) extended the basic SHAM model to include four additional parameters. They showed that by including these additional parameters, the extended SHAM (SHAMe) model was able to accurately reproduce galaxy clustering in both real and redshift space in a state-of-the-art hydrodynamical simulation. They then additionally showed that the SHAMe model was able to simultaneously describe galaxy–galaxy lensing and galaxy clustering in both hydrodynamic simulations (S. Contreras et al. 2023a, 2024) and in real galaxy observations (S. Contreras et al. 2023c).

The five parameters included in the SHAMe model are

$$[\sigma,\ t_{\rm merger},\ f_{\rm k,c+s},\ f_{\rm k,c-s},\ \beta]. \tag{1}$$

In this case, σ is the scatter between $V_{\rm peak}$, the peak maximum circular velocity of a dark matter subhalo during its evolution, and $M_\star$, the stellar mass or luminosity of the associated galaxy. $t_{\rm merger}$ regulates the number of orphan galaxies in the simulation by removing galaxies that have been orphans for a large number of dynamical times. Orphan galaxies are galaxies that are no longer associated with a dark matter subhalo, as the mass of the dark matter subhalo has fallen below the resolution of the simulation. Including orphan galaxies is important to reproduce the small-scale galaxy clustering pattern (Q. Guo & S. White 2014).

The parameters $f_{\rm k,c+s}$ and $f_{\rm k,c-s}$ regulate the amount of galaxy assembly bias in the sample. Galaxy assembly bias (D. J. Croton, L. Gao & S. D. M. White 2007) is the impact of the evolutionary history of host haloes on the clustering of their associated galaxies. Specifically, $f_{\rm k,c+s}$ and $f_{\rm k,c-s}$ represent the sum and the difference between the amount of galaxy assembly bias added to central (c) and satellite (s) galaxies, and they re-order the $V_{\rm peak}$–$M_\star$ relation for the galaxies while preserving the original scatter σ. If these parameters are positive/negative, the model will assign a larger/smaller stellar mass or luminosity to galaxies with a larger linear galaxy bias, resulting in a positive/negative correlation. If they are equal to zero the stellar masses or luminosities are randomly re-assigned. The bias-per-object is calculated using the method from A. Paranjape, O. Hahn & R. K. Sheth (2018) and is computed independently for centrals and satellites, so the satellite fraction is preserved. A deeper explanation of this implementation can be found in S. Contreras, R. E. Angulo & M. Zennaro (2021a).

The final parameter is β, which sets the time-scale for how long satellite galaxies survive within their host halo. Satellite galaxies progressively lose mass and luminosity over time due to dynamical friction, so eventually no longer have the minimum mass or luminosity required to enter our sample, or even completely disappear

into the intra-cluster medium. Satellite galaxies should therefore be removed if they have been satellites for a long time. For further details about the SHAMe parameters, see S. Contreras et al. (2021c).

2.2 Galaxy clustering and galaxy–galaxy lensing

The SHAMe formalism can be applied to the subhalo catalogues of gravity-only simulations to populate them with galaxies. Summary statistics of the galaxy clustering and galaxy–galaxy lensing can then be computed from the distribution of these galaxies.

The galaxy clustering statistic we use in this work is the projected correlation function $w_{\rm p}(r_{\rm p})$, which is found by integrating the three-dimensional galaxy correlation function $\xi_{\rm gg}(r_{\rm p}, r_\pi)$ over the line-of-sight separation r_π,

$$w_{\rm p}(r_{\rm p}) = 2\int_0^{r_{\pi,\rm max}} \xi_{\rm gg}(r_{\rm p}, r_\pi)\,{\rm d}r_\pi\ , \tag{2}$$

where $r_{\rm p}$ is the projected separation between two galaxies and $r_{\pi,\rm max}$ is the maximum integration range. We utilize CORRFUNC[2] (M. Sinha & L. H. Garrison 2020) to compute $w_{\rm p}(r_{\rm p})$, and use $r_{\pi,\rm max} = 60$ Mpc h^{-1} to match the measurements from Galaxy And Mass Assembly (GAMA) used in this work (see Section 3). We include the effect of redshift-space distortions in the clustering, but they only have a small impact due to our value of $r_{\pi,\rm max}$.

The galaxy–galaxy lensing statistic we use in this work is the excess surface density profile $\Delta\Sigma(r_{\rm p})$, where we subtract the projected surface mass density $\Sigma(r_{\rm p})$ from the mean surface mass density within a given projected radius $\overline{\Sigma}(\leq r_{\rm p})$,

$$\Delta\Sigma(r_{\rm p}) = \overline{\Sigma}(\leq r_{\rm p}) - \Sigma(r_{\rm p})\ . \tag{3}$$

The projected surface mass density $\Sigma(r_{\rm p})$ is related to the galaxy–matter correlation function $\xi_{\rm gm}(r_{\rm p}, r_\pi)$ by

$$\Sigma(r_{\rm p}) = 2\Omega_{\rm m}\rho_{\rm crit}\int_0^{r_{\pi,\rm max}} \xi_{\rm gm}(r_{\rm p}, r_\pi){\rm d}r_\pi\ , \tag{4}$$

where $\rho_{\rm crit}$ is the critical density of the Universe. The mean surface mass density within a given projected radius $\overline{\Sigma}(\leq r_{\rm p})$ is given by

$$\overline{\Sigma}(\leq r_{\rm p}) = \frac{2}{r_{\rm p}^2}\int_0^{r_{\rm p}} \Sigma(R')R'{\rm d}R'\ . \tag{5}$$

We again utilize CORRFUNC to compute $\Delta\Sigma(r_{\rm p})$, and integrate out to $r_{\pi,\rm max} = 233$ Mpc h^{-1} to match the measurements from KiDS-1000 (see Section 3). To compute $\xi_{\rm gm}$, we extract a subsampled version of the dark matter density field from the gravity-only simulation, which we then correlate with the distribution of galaxies produced by the SHAMe formalism. A dilution factor of $\sim 1/3000$ was previously found to produce $\Delta\Sigma(r_{\rm p})$ measurements with sub- per cent precision (S. Contreras et al. 2023a).

2.3 SHAMe emulator

We created an emulator to speed up the computation of galaxy clustering and galaxy–galaxy lensing using the procedure described in S. Contreras et al. (2023b). Here, we briefly summarize the main steps in building the emulator.

(i) We begin by running five gravity-only simulations with varying cosmology (as described in S. Contreras et al. 2020). These simulations have 3072^3 particles over a $(1024\ h^{-1}\,{\rm Mpc})^3$ volume, which is roughly a mass resolution of 3–4 $\times\ 10^9\ h^{-1}\,{\rm M}_\odot$.[3] The simulations were run using the fixed initial condition technique by R. E. Angulo & A. Pontzen (2016), which significantly reduces the effect of cosmic variance on a simulation, at least for second-order statistics.

Table 1. Parameter ranges of the SHAMe emulator; see Section 2.1 for details of the SHAMe parameters. These ranges are also the fiducial top-hat prior ranges used in our analysis of GAMA galaxy clustering and KiDS-1000 galaxy–galaxy lensing with SHAMe.

Parameter	Prior
σ_8	[0.65, 0.9]
$\Omega_{\rm m}$	[0.23, 0.4]
$\Omega_{\rm b}$	[0.04, 0.06]
$n_{\rm s}$	[0.92, 1.01]
h	[0.64, 0.8]
$\sigma\ \log {\rm M}$	[0.1, 1.8]
$\log t_{\rm merger}$	[−1.5, 1.2]
$f_{\rm k,c+s}$	[−1.5, 1.5]
$f_{\rm k,c-s}$	[−1.5, 1.5]
β	[0.0, 1.0]

(ii) We scaled these five simulations to 10 000 distinct cosmologies by employing the scaling technique of R. E. Angulo & S. D. M. White (2010). The upper part of Table 1 shows the cosmological parameters we scaled and the range within which we varied them. For each cosmology, we generate an average of eight snapshots between $z = 0$ and $z = 2$. As demonstrated in S. Contreras et al. (2020) and S. Contreras et al. (2023b), the scaled simulations precisely reproduce the mass distribution of the desired cosmology, needing only 6 min to scale.

(iii) We populate each of the $\sim$ 80 000 scaled snapshots with two SHAMe mocks. The SHAMe parameters used, as well as the range within which they were varied, are shown in the lower part of Table 1. These ranges were chosen based on the model's performance in fitting galaxy clustering and galaxy–galaxy lensing simulations (S. Contreras et al. 2023a, b, 2024) and observations (S. Contreras et al. 2023c). For this work we have assumed the sum of the neutrino masses to be equal to zero.

(iv) For each mock, we compute the galaxy correlation function $\xi_{\rm gg}(r_{\rm p}, r_\pi)$ up to a scale of $r_{\pi,\rm max} = 100\ h^{-1}$ Mpc, and the galaxy–matter correlation function $\xi_{\rm gm}(r_{\rm p}, r_\pi)$ up to a scale of $r_{\pi,\rm max} = 240\,h^{-1}$Mpc for eight galaxy samples with number densities ranging from ${\rm n_{den}} = 10^{-4}$ to $10^{-2.25}\ h^3\,{\rm Mpc}^{-3}$. We then compute $w_{\rm p}(r_{\rm p})$ and $\Delta\Sigma({\rm r_p})$ using the steps described in the previous section, up to a maximum scale of 60 and 233 h^{-1}Mpc, respectively. We computed correlation functions with larger values of $\rm r_{\pi,max}$ so that we could use these calculations for future observational samples.

(v) Using over 1000 000 projected correlation functions and galaxy–galaxy lensing calculations, we created an emulator that can predict these statistics as a function of the cosmological and SHAMe parameters, as well as the sample redshift and galaxy number density. The emulator was built using a feed-forward neural network, similar to the one described in R. E. Angulo et al. (2021). The architecture used consists of two fully connected hidden layers, each with 200 neurons, and a rectified linear unit activation function, with each statistic represented by its own network. The neural networks were trained with the Keras front-end of the TensorFlow library (M. Abadi

[2] https://github.com/manodeep/Corrfunc

[3] The mass resolution can vary slightly between the simulations, due to their differing cosmologies.

et al. 2015). We applied the Adam optimization algorithm with a learning rate of 0.001 and a mean squared error loss function. Evaluating one of these emulators takes ~ 40 ms on a laptop and ~ 1.6 s to evaluate 100 000 samples (it is more efficient to evaluate the data in larger groups).

The measurements of $w_{\rm p}$ and $\Delta\Sigma$ made from the real data depend implicitly on the fiducial cosmology used to transform redshifts into distances. This procedure is mimicked in the galaxy clustering and galaxy–galaxy lensing measurements made from the simulations used to construct the emulator, assuming that the observer uses a fiducial cosmological model (different from that of the simulation). We adopt the procedure described in J. U. Lange et al. (2019), where these effects are incorporated by modifying the box geometry and appropriately adjusting the coordinate system. In doing this, we assumed a fixed *Planck*-like cosmology, with $\Omega_m = 0.314$. This is slightly different from the cosmology assumed in the real data ($\Omega_m = 0.3$) (A. Dvornik et al. 2023), but we verified that the difference is negligible given the sensitivity of our measurements (the effect is less than 7 per cent of the statistical uncertainties).

3 DATA

In this work we use galaxy clustering measurements from the final data release of the GAMA (S. P. Driver et al. 2022a), and galaxy–galaxy lensing measurements from the fourth data release of the Kilo-Degree Survey (KiDS-1000; K. Kuijken et al. 2019). These two data sets are described below. The lens sample used for galaxy–galaxy lensing is based on the KiDS Bright sample (M. Bilicki et al. 2021), and was designed to match the selection of the GAMA sample. We will thus assume that these lenses and the GAMA sample used for galaxy clustering have the same properties and are described by the same SHAMe parameters. This allows us to avoid the significant impact of photometric redshift uncertainties in the galaxy clustering measurements.

3.1 Kilo Degree Survey

The KiDS is an imaging survey carried out at the European Southern Observatory VLT Survey Telescope in the $ugri$ broad-band filters. The data cover a sky area of 1347 deg^2 (K. Kuijken et al. 2019; A. H. Wright et al. 2024) and are complemented by fully overlapping infrared photometry in the $ZYJHK_s$ bands from the VISTA Kilo-degree INfrared Galaxy (VIKING) survey (A. Edge et al. 2013). KiDS was specifically designed for weak gravitational lensing science and the imaging data reflect this in their excellent seeing and well-behaved point-spread function. The nine-band photometry also assists greatly with the determination of photometric redshift estimates (photo-z) for the galaxy sample. The r-band data, used for the estimation of galaxy shapes, were obtained within strict observing condition limits and reach a median 5σ limiting magnitude of 24.8 and median seeing of 0.7 arcsec.

We use measurements of the galaxy–galaxy lensing signal, based on KiDS-1000 data, as presented in A. Dvornik et al. (2023) and detailed here as well. The sample of source galaxies used as gravitational shear tracers is detailed in B. Giblin et al. (2021), with their photometric redshift estimates described in H. Hildebrandt et al. (2021). The source sample number density is 6.17 galaxies/arcmin^2 and spans a photo-z range of $0.1 < z_B < 1.2$, where z_B is the estimated photometric redshift. The lens galaxies used as density tracers are selected from the KiDS Bright sample (M. Bilicki et al. 2021). This sample is designed to match the selection of the GAMA galaxy sample (see Section 3.2) for which spectroscopic redshift information is available. The GAMA sample is then used as training data for estimating machine-learning-based photometric redshifts over the KiDS-1000 area. The resulting lens sample benefits from accurate photo-z estimates, with a mean offset of $\delta z = 5 \times 10^{-4}$ and a standard mean absolute deviation of $\sigma_z = 0.018(1+z)$. Stellar mass estimates for this sample are also available using the spectral energy density template-fitting code LEPHARE (S. Arnouts et al. 1999; O. Ilbert et al. 2006). See M. Bilicki et al. (2021) for further details.

The lens galaxy sample is split into six volume-limited stellar mass bins, the details of this procedure are described in A. Dvornik et al. (2023). We only include the highest four stellar mass bins in our analysis, as the lowest two bins are currently outside the maximum number density of our SHAMe emulator (see Section 3.4). We plan to extend the number density range of the SHAMe emulator in the next version. The stellar mass bin boundaries used in this analysis are [9.95, 10.25, 10.5, 10.7, 11.3] in units of $\log(M_\star/h^{-2}\,{\rm M}_\odot)$ and the measured $\Delta\Sigma$ are shown in Fig. 5.

3.2 Galaxy And Mass Assembly survey

To complement the galaxy–galaxy lensing measurements and break degeneracies between cosmological and SHAMe parameters, we make use of projected galaxy clustering measurements. However, the presence of un-modelled photometric redshift uncertainties makes attempting this measurement with the KiDS Bright sample difficult. This was previously identified in A. Dvornik et al. (2023) and led to the introduction of an additional photometric dilution parameter. We also found it challenging to obtain a good fit to the KiDS Bright photometric clustering with the SHAMe model used in this study. We therefore decided to perform galaxy clustering measurements using the GAMA galaxy sample, which we treat as being described by the same SHAMe parameters as the KiDS Bright sample. Note that the galaxy–galaxy lensing measurements are significantly less affected by photometric errors (A. Dvornik et al. 2023).

The GAMA survey (S. P. Driver et al. 2011) is a spectroscopic survey carried out using the AAOmega spectrograph at the Anglo-Australian Telescope (AAT) covering approximately 250 deg^2 of the sky in five patches. Of these, we use the three equatorial patches (G09, G12, and G15) that have a homogeneous target selection with a Petrosian r-band magnitude limit of $r^{\rm Petro} < 19.8$ mag and fully overlap with the KiDS survey. The survey's strategy prioritized completeness, involving multiple passes over the same sky area. We use data from the final data release (GAMA III; S. P. Driver et al. 2022b), which achieves a completeness of 95 per cent with a limiting magnitude of $r < 19.72$. We make use of stellar mass measurements from the `StellarMassesGKVv24` (E. N. Taylor et al. 2011) Data Management Unit (DMU) and local-flow corrected redshifts (`Z_TONRY` column) from the `DistancesFramesv14` DMU (I. K. Baldry et al. 2012).

The KiDS Bright sample, from which our lens galaxies are chosen, has been designed to match the GAMA galaxies as well as possible. An exact match is difficult due to GAMA having been selected on Petrosian r-band magnitude (see M. Bilicki et al. 2021, for details). The differences between these two samples were recently studied in C. Georgiou et al. (2025) and are present mostly at the tail end of the redshift distribution. Given that our lens sample is selected to be volume-limited and does not extend to redshifts beyond 0.4, this mismatch is not expected to be significant. Therefore, we treat these two samples as containing the same type of galaxies.

We apply the stellar mass and redshift cuts from the KiDS Bright sample to the GAMA sample and estimate the projected correlation function using equation (2), where $\xi_{\rm gg}$ is now the estimated galaxy correlation function. We use 10 logarithmically spaced $r_{\rm p}$ bins between 0.15 and 25 Mpc h^{-1}, and take $r_{\pi,\rm max} = 60\,{\rm Mpc}\,h^{-1}$ binned in 30 linearly spaced bins. We chose the range of r_p to mimic the range shown in A. Dvornik et al. (2023) who previously study the clustering and lensing of KiDS-1000. Correlation functions are estimated using TREECORR[4] (M. Jarvis, G. Bernstein & B. Jain 2004) and the measured $w_{\rm p}$ are shown in Fig. 5. We use the GAMA `Randoms v02` DMU (D. J. Farrow et al. 2015) – specifically designed for the GAMA survey[5] – as the random points catalogue. Given the bright magnitude cut and high completeness of GAMA, this random catalogue does not need to account for spatially varying observational systematics, but models carefully the radial selection function of the data.

3.3 Covariance

We use the analytic covariance detailed in A. Dvornik et al. (2023) (and previously validated by H. Johnston et al. 2019) for the KiDS-1000 galaxy–galaxy lensing measurements, and compute a jackknife covariance using 12 patches for the GAMA galaxy clustering data. The jackknife patches, which are approximately 15 deg^2 in area, were defined using KMEANS-RADEC.[6] We do not include cross-correlations between the different galaxy clustering stellar mass bins, as they do not bring in significant additional information, and obtaining a sufficiently accurate covariance would have required a much larger set of jackknife realizations. Our covariance matrix also assumes no correlation between the KiDS-1000 $\Delta\Sigma$ measurements and the GAMA $w_{\rm p}$ measurements. A. Dvornik et al. (2023) found the correlation between these observables within KiDS itself to be small, and we expect them to become negligible when switching to GAMA clustering, given GAMA only covers approximately 20 per cent of the KiDS sky area (A. H. Wright et al. 2024).

3.4 Cumulative number densities

In A. Dvornik et al. (2023) the stellar mass function is an output of the galaxy–halo connection modelling, which is the analytic Conditional Stellar Mass Function formalism (X. Yang, H. J. Mo & F. C. v. d. Bosch 2008; M. Cacciato et al. 2009, 2013; S. More et al. 2013; F. C. van den Bosch et al. 2013; L. Wang et al. 2013). This means that the stellar mass function can be jointly analysed, along with galaxy clustering and galaxy–galaxy lensing. In SHAMe, the stellar mass function acts as an input to the modelling. Normally, the specific form of the stellar mass function has very little effect (S. Contreras et al. 2021b). However, when the galaxy sample is binned in stellar mass, it becomes more important because the SHAMe emulator requires a cumulative number density input.

To model the galaxy clustering in a particular stellar mass bin we first convert the stellar mass bin edges ($M_{\star 1}$, $M_{\star 2}$ where $M_{\star 1} < M_{\star 2}$) to cumulative number densities (n_1, n_2 where $n_1 > n_2$) using the cumulative stellar mass function. We are then able to use the SHAMe emulator to compute the galaxy clustering $w_{\rm p}$ for two galaxy samples where the minimum stellar mass corresponds to each of the bin edges,

$$\begin{aligned} w_{\rm p}(M_\star > M_{\star 1}) &= w_{\rm p}(n = n_1) \\ w_{\rm p}(M_\star > M_{\star 2}) &= w_{\rm p}(n = n_2)\,. \end{aligned} \tag{6}$$

Then, from these, we estimate the galaxy clustering within a given stellar mass bin,

$$\begin{aligned} w_{\rm p}(M_{\star 1} < M_\star < M_{\star 2}) \simeq\ & w_{\rm p1}\left(\frac{n_1}{n_1 - n_2}\right)^2 \\ & + w_{\rm p2}\left(\frac{n_2}{n_1 - n_2}\right)^2 \\ & - 2\sqrt{w_{\rm p1} w_{\rm p2}}\left(\frac{n_1 n_2}{(n_1 - n_2)^2}\right), \end{aligned} \tag{7}$$

where $w_{\rm p1} = w_{\rm p}(n = n_1)$, $w_{\rm p2} = w_{\rm p}(n = n_2)$, and $n_1 > n_2$. The derivation of this expression can be found in Appendix B. For galaxy–galaxy lensing $\Delta\Sigma$, the computation is even simpler. We compute

$$\begin{aligned} \Delta\Sigma(M_\star > M_{\star 1}) &= \Delta\Sigma(n = n_1) \\ \Delta\Sigma(M_\star > M_{\star 2}) &= \Delta\Sigma(n = n_2)\,, \end{aligned} \tag{8}$$

using the SHAMe emulator. Then compute the galaxy–galaxy lensing within a given stellar mass bin,

$$\Delta\Sigma(M_{\star 1} < M_\star < M_{\star 2}) = \left(\frac{n_1}{n_1 - n_2}\right)\Delta\Sigma_1 - \left(\frac{n_2}{n_1 - n_2}\right)\Delta\Sigma_2, \tag{9}$$

where $\Delta\Sigma_1 = \Delta\Sigma(n = n_1)$, $\Delta\Sigma_2 = \Delta\Sigma(n = n_2)$, and $n_1 > n_2$. We validated these relations using the TNG300 hydrodynamic simulation (D. Nelson et al. 2019), and found that for $w_{\rm p}$ the differences were less than 1 per cent across all scales and that for $\Delta\Sigma$ the relation was exact.

To convert the stellar mass bin edges to cumulative number densities, we require the cumulative stellar mass function of our galaxy sample. While this is easily accessible for simulated data, it is a lot more complex to obtain for real data, due to difficulties in accurately defining the volume of a galaxy survey. Therefore, in this work, we compute the cumulative number densities from the cumulative stellar mass function of TNG300, instead of from GAMA or KiDS-1000 data. Fig. 1 shows a comparison between the TNG300, GAMA (S. P. Driver et al. 2022a), and KiDS-1000 (A. Dvornik et al. 2023) differential stellar mass functions, where the grey dashed lines indicate the stellar mass bin boundaries used in A. Dvornik et al. (2023) and the grey shaded region indicates the stellar mass bins outside the current number density range of our SHAMe emulator. We find good agreement between the three differential stellar mass functions, and in Section 5.1 show that our fiducial analysis is resilient to our choice of cumulative number density inputs. A future extension of this work would be to adapt the SHAMe emulator to work with differential number densities, which are more accessible for real data, and then include these number densities with an associated uncertainty in the analysis.

3.5 Likelihood

To obtain constraints on the free parameters of our model, we assume a Gaussian likelihood of the form

$$-2\log p(\mathbf{d}|\vec{\theta}) \equiv \chi^2 = (\mathbf{d} - \mathbf{t}(\vec{\theta}))^T \mathbf{C}^{-1} (\mathbf{d} - \mathbf{t}(\vec{\theta})), \tag{10}$$

where $\mathbf{d}$ is our data vector, $\mathbf{t}$ is the theoretical prediction for $\mathbf{d}$, dependent on the free model parameters $\vec{\theta}$, and $\mathbf{C}$ is the covariance

[4] http://rmjarvis.github.io/TreeCorr

[5] The random catalogue we used was built for GAMA II, but it should also be representative of the GAMA III sample since the two data releases have the same target selection in the equatorial regions.

[6] https://github.com/esheldon/kmeans-radec

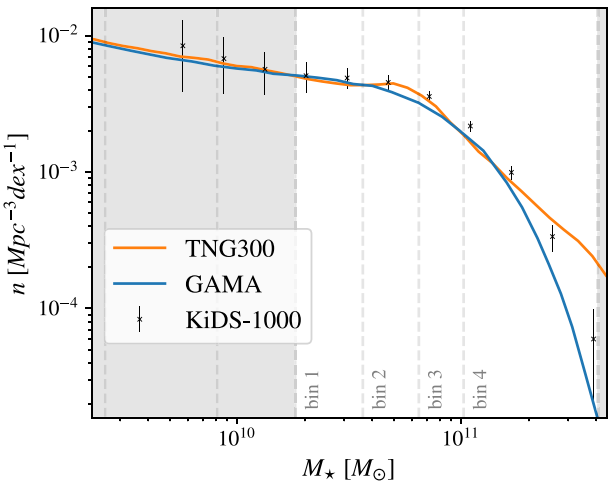

Figure 1. Differential stellar mass function from TNG300 compared to GAMA (S. P. Driver et al. 2022a) and KiDS-1000 (A. Dvornik et al. 2023). The dashed lines indicate the stellar mass bin boundaries, which are required as inputs to the SHAMe emulator. We do not include the bins in the shaded region, as they fall outside the range of the emulator.

matrix of our measurements. The measurements and covariance are described above.

Specifically, we use measurements of the projected correlation function w_p of galaxies in four stellar mass bins, as well as their cross-correlation with gravitational shear $\Delta\Sigma$, from a single sample of source galaxies. The data vector $\mathbf{d}$ thus comprises four different estimates of w_p and $\Delta\Sigma$, one per stellar mass bin. We do not consider cross-correlations between mass bins. The measurements span transverse separations in the range $0.15\,\mathrm{Mpc}\,h^{-1} < r_p < 25\,\mathrm{Mpc}\,h^{-1}$. In our fiducial analysis we use this full range for w_p, but impose a scale cut of $r_\mathrm{p} < 1.4\,\mathrm{Mpc}\,h^{-1}$ for the $\Delta\Sigma$ data, to avoid the potential impact of baryonic feedback, which is not currently included in our model. We determine this value by looking at the expected impact of baryonic effects following S. Contreras et al. (2024). We study the dependence of our results on this choice (see Section 5.2). Our fiducial data vector contains a total of 64 elements.

The free parameters of the model are the five ΛCDM cosmological parameters (σ_8, Ω_m, Ω_b, n_s, h), as well as five SHAMe parameters, which are described in Section 2.1. These parameters and their associated priors are shown in Table 1. We evaluate the emulator (see Section 2.3) at the median redshift of each stellar mass bin [0.18, 0.22, 0.27, 0.32], and assume that the SHAMe parameters do not evolve with redshift or stellar mass. This assumption could be explored further in future work. We do not include intrinsic alignments or lens galaxy magnification in our model as A. Dvornik et al. (2023) found them to have a negligible impact on both w_p and $\Delta\Sigma$. We sample the parameter space using NAUTILUS[7] (J. U. Lange 2023) with 3000 live points.

4 VALIDATION ON SIMULATED SAMPLE

Before applying our methodology to KiDS-1000 and GAMA data, we validated it on a simulated sample from the TNG300 hydrodynamic simulation. This was to determine whether we were able to obtain robust cosmological constraints.

[7] https://github.com/johannesulf/nautilus

We constructed our simulated sample by selecting galaxies from the redshift zero snapshot of TNG300 with stellar masses within the stellar mass ranges of the real data. This gave us four simulated galaxy samples, from which we computed the galaxy clustering w_p and galaxy–galaxy lensing $\Delta\Sigma$ using the same methodology described in Section 2.2, except for one difference. When creating the simulated $\Delta\Sigma$ from TNG300, instead of extracting only the dark matter field, as we do for the emulator in Section 2.2, which uses gravity-only simulations, we also extracted the density fields for stars and gas. This means that the simulated $\Delta\Sigma$ from TNG300 includes the impact of baryons, but that the emulator for $\Delta\Sigma$ does not include them. A future extension to this work would be to include baryonic effects in the SHAMe emulator following the techniques introduced in G. Aricò et al. (2021) and M. Zennaro et al. (2025).

The simulated data can be seen in Fig. 2. They are very similar to the real GAMA and KiDS-1000 data, but do not match exactly for a few reasons. First, the simulated data are computed at redshift zero instead of the median redshift of each stellar mass bin, which are [0.18, 0.22, 0.27, 0.32]. This results in a slight discrepancy between the real and simulated data. Secondly, the underlying cosmology of the TNG300 sample may be slightly different from that of the real Universe. Thirdly, there may be some small differences in how stellar masses are computed for the real and simulated data, as well as some possible incompleteness at low stellar masses. Finally, the galaxy formation physics in TNG300 is likely not representative of the real Universe, and the clustering data were not used to calibrate the sub-grid physics. Despite these differences, the simulated data vector is very close to the real data vector, so it provides a good test for our methodology.

After constructing the simulated galaxy clustering and galaxy–galaxy lensing data vectors from TNG300 we analysed them in exactly the same way as the real data; using the same covariance (Section 3.3), cumulative number density inputs (Section 3.4), and likelihood (Section 3.5). Fig. 3 shows our marginal posterior constraints on S_8 and Ω_m for two variations of our analysis. The blue contour shows our fiducial case where we remove scales of $\Delta\Sigma$, where $r_\mathrm{p} < 1.4\,\mathrm{Mpc}\,h^{-1}$, as we do not model baryonic effects, and the green contour shows an extended analysis where we include all scales of $\Delta\Sigma$. For a detailed discussion of the impact of baryons on our analyses, see Section 5.2. The dashed lines indicate the input cosmology of TNG300, and we are able to recover the input cosmology of the simulation within 1σ in both cases.

Fig. 2 shows the best-fitting galaxy–galaxy lensing and clustering predictions for our fiducial analysis (blue), and for the extended analysis including smaller scales in $\Delta\Sigma$ (green). These predictions were estimated for the maximum a posteriori parameter values, which align with the marginal distributions in Fig. 3. Both cases provide a good fit to the data, with the extended analysis providing a better fit for the small-scale galaxy–galaxy lensing, as expected. Since we use the real data covariance when analysing our simulated data vectors, the corresponding chi-squared values are meaningless as an absolute goodness-of-fit metric.

5 RESULTS

We present cosmological constraints for a combined analysis of GAMA galaxy clustering and KiDS-1000 galaxy–galaxy lensing analysed using SHAMe to model the galaxy–halo connection. Fig. 4 shows our main result, constraints on Ω_m and $S_8 \equiv \sigma_8\sqrt{\Omega_\mathrm{m}/0.3}$. We show our fiducial result (blue contour), as well as an extended analysis that includes all scales of galaxy–galaxy lensing (green contour). Our results are compared to the *Planck* TT,TE,EE + lowE

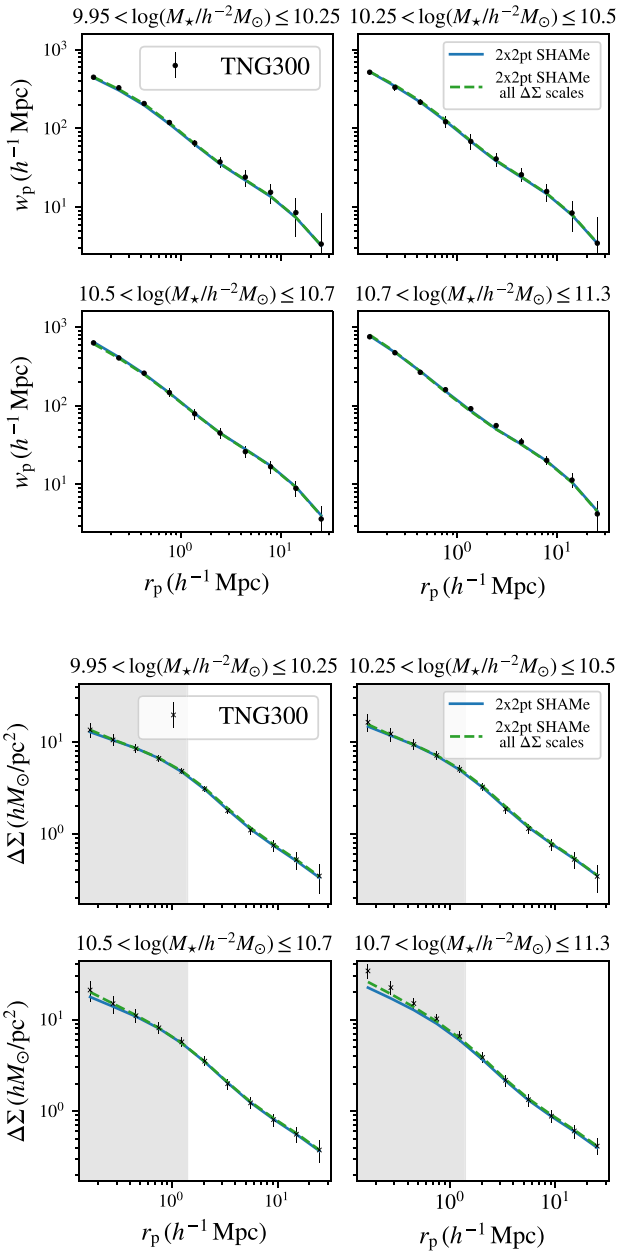

Figure 2. TNG300 galaxy clustering (top) and TNG300 galaxy–galaxy lensing (bottom) for each of the four stellar mass bins used in this work. The solid blue line shows the best fit when analysing the joint data vector with SHAMe, where the galaxy–galaxy lensing data in the grey shaded region are not included, and the green dashed line shows the best fit when all scales of the galaxy–galaxy lensing are included in the data vector.

CMB result (orange contour, Planck Collaboration VI 2020), and a precursor analysis with KiDS-1000 (red contour, A. Dvornik et al. 2023).

5.1 Fiducial analysis

In our fiducial analysis (Fig. 4, blue contour) we find $S_8 = 0.793^{+0.025}_{-0.024}$ and $\Omega_m = 0.260^{+0.027}_{-0.015}$. These results are consistent with *Planck*, with a lower value of S_8 that is in agreement at the 1.7σ level (computed as the 1D difference between the two predictions), and a slightly larger difference for Ω_m values (also shifted to lower values). We are

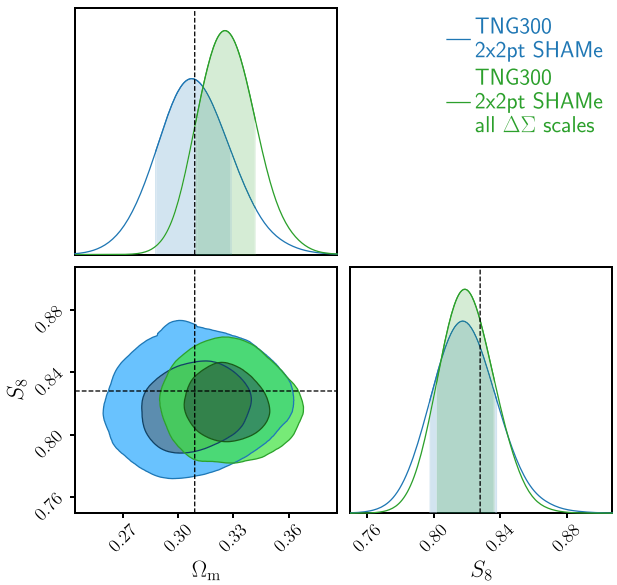

Figure 3. Marginalized posterior constraints on S_8 and Ω_m for TNG300 galaxy clustering and galaxy–galaxy lensing using SHAMe (blue) and the same analysis without scale cuts in the galaxy–galaxy lensing (green). We recover the TNG300 input cosmology (dashed lines) within 1σ, where the covariance matches the covariance used in the real data analysis.

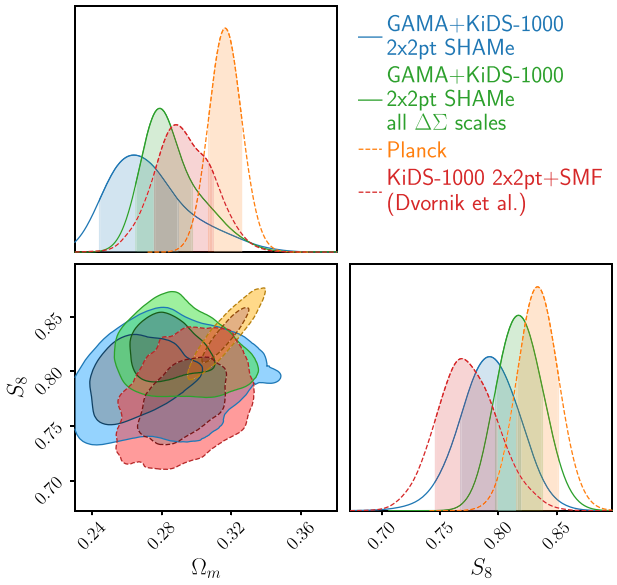

Figure 4. Marginalized posterior constraints on S_8 and Ω_m for GAMA galaxy clustering and KiDS-1000 galaxy–galaxy lensing using SHAMe (blue) and the same analysis without scale cuts in the galaxy–galaxy lensing (green). For comparison, we show CMB results from *Planck* (Planck Collaboration VI 2020, orange dashed) and results for KiDS-1000 galaxy clustering and galaxy–galaxy lensing using an analytic conditional stellar mass function to describe the galaxy–halo connection (A. Dvornik et al. 2023, red dashed). The results are consistent, with SHAMe (this work) giving a slightly higher value of S_8, particularly when all scales are included in the galaxy–galaxy lensing.

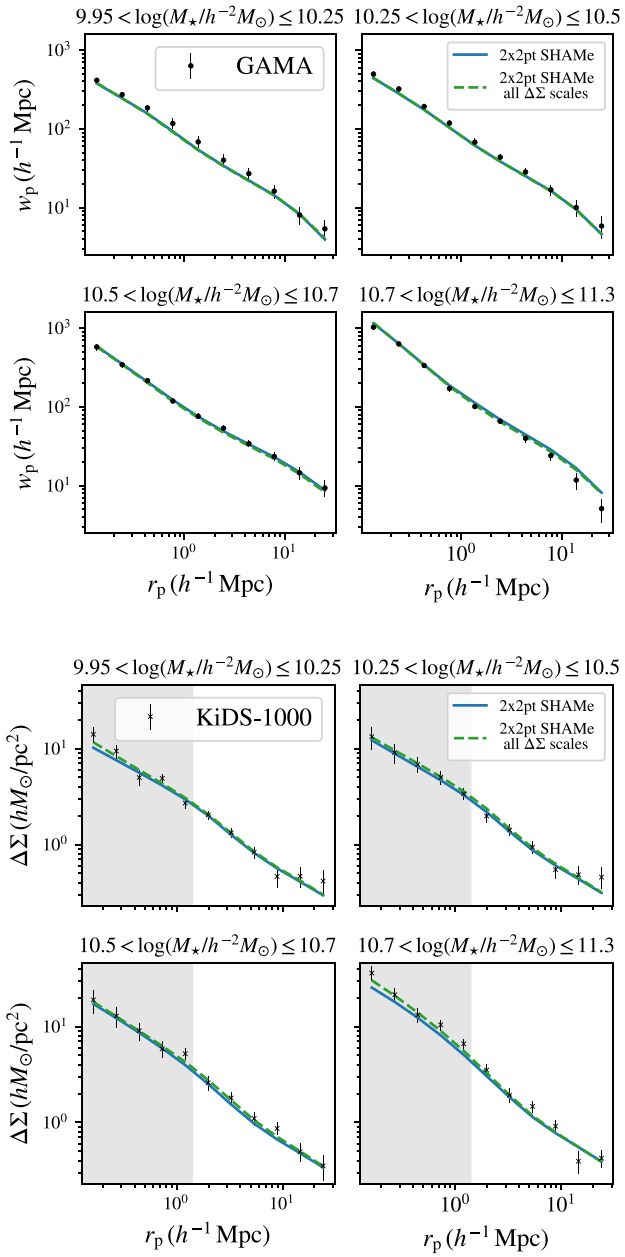

Figure 5. GAMA galaxy clustering (top) and KiDS-1000 galaxy–galaxy lensing (bottom) for each of the four stellar mass bins used in this work. The solid line shows the best fit when analysing the joint data vector with SHAMe, where the galaxy–galaxy lensing data in the shaded region are not included in order to avoid the impact of baryonic effects (Fig. 4, blue contour). The dashed line shows the best fit when all scales of the galaxy–galaxy lensing are included in the data vector (Fig. 4, green contour).

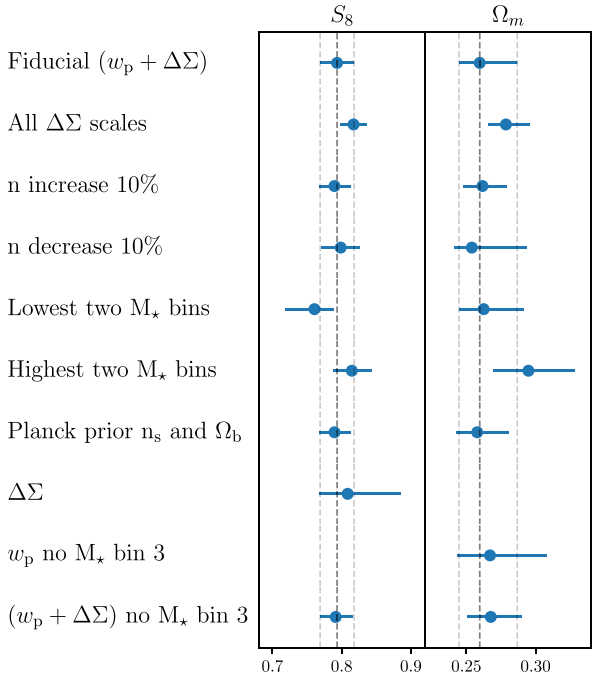

Figure 6. S_8 and Ω_m marginal constraints for variations of our fiducial joint analysis of GAMA galaxy clustering and KiDS-1000 galaxy–galaxy lensing using SHAMe. We find consistency between our analysis and all of the variations shown.

also able to constrain all five SHAMe parameters (see Section 5.3 for details). We find a good fit to the data with a chi-squared value of 74.2 and a chi-squared per degree of freedom of 1.37, where we use a simple estimate of the number of degrees of freedom as the number of data points minus the number of constrained parameters, in this case 64–10. The associated p-value is 0.036, which we consider to be adequate (the model is able to explain the data at less than 2σ). These values are similar to the ones obtained using the small scales of the galaxy–galaxy lensing (1.28 and 0.051, receptively), which is particularly impressive, since we are not fitting those scales. Our best-fitting clustering and galaxy–galaxy lensing, calculated using the maximum posterior values of our fiducial result, can be seen in Fig. 5 (blue line). We show the best-fitting galaxy–galaxy lensing extrapolated to the full range of r_p scales, but we only compute this best fit using the data outside of the grey shaded region in order to remove baryonic effects. The current version of the SHAMe emulator does not model baryonic effects in $\Delta\Sigma(r_p)$, so in our fiducial case, we remove scales where $r_p < 1.4\,\mathrm{Mpc}\,h^{-1}$. See Section 5.2 for further details about the impact of baryons. In our fiducial case, the model is able to describe the data on all scales, even those not used to constrain it, which emphasizes the physically motivated nature of the SHAMe model. We are also able to simultaneously reproduce the galaxy clustering and galaxy–galaxy lensing measurements across all the stellar mass bins, which SHAMe was not originally designed to do.

In Fig. 6 we quantify the impact of various analysis choices on our fiducial constraints. Any differences in the recovered value of S_8 compared to the fiducial result are quantified in terms of the metric $(S_8^{\mathrm{fid}} - S_8^{\mathrm{var}})/\sigma_{S_8^{\mathrm{var}}}$. We discuss extending the analysis to all $\Delta\Sigma$ scales and the impact of baryons in detail in Section 5.2.

In our fiducial analysis, we use the cumulative number densities from the TNG300 simulation as inputs for the SHAMe emulator, instead of those from GAMA or KiDS-1000 (see Section 3.4). We assess the impact of this choice by increasing/decreasing the SHAMe number density inputs by 10 per cent, motivated by Fig. 1, and find shifts of $0.16\sigma/0.19\sigma$ in S_8, demonstrating that our analysis is robust to this choice. We check that our results are consistent across the stellar mass bins by analysing the two lowest and two highest stellar mass bins separately. We find broad consistency between the two sets of bins, with shifts of $1.16\sigma/0.77\sigma$ in S_8 for the two lowest/highest bins, respectively. However, these variations are limited by the number of data points compared to the number of free parameters, and the majority of the constraining power for the five

SHAMe parameters comes from the two highest stellar mass bins. Therefore, even though we find broad consistency across the stellar mass bins, the power of the analysis comes from combining a range of stellar masses. We also check the impact of adding a *Planck* prior to the unconstrained cosmological parameters, n_s and Ω_b, and find a small shift of 0.16σ in S_8.

In the last three rows of Fig. 6, we illustrate the power of combined analyses of galaxy clustering and galaxy–galaxy lensing. When analysing $\Delta\Sigma$ alone, we are only able to place a wide constraint on S_8, and when analysing w_p alone, we are only able to place a wide constraint on Ω_m. However, combining the two, we can constrain both S_8 and Ω_m with greater precision. For a discussion of the power of combining w_p and $\Delta\Sigma$ in the context of the SHAMe parameters, see Section 5.3. When initially analysing w_p alone we found a significant constraint on S_8, which was inconsistent with our fiducial result, and is not expected using only galaxy clustering data. We found that this constraint disappeared when we removed stellar mass bin 3, $10.5 < \log(M_\star/h^{-2}\,M_\odot) \leq 10.7$, and even if we just removed the large scales of bin 3, where $r_{max} > 1.5\,h^{-1}$ Mpc (see Appendix A). We therefore suspect the presence of an uncontrolled systematic effect in the large scales of bin 3. To avoid confirmation bias, we did not remove w_p bin 3 from our fiducial joint data vector. However, in the final row of Fig. 6 we show that our fiducial analysis is only negligibly affected when stellar mass bin 3 is removed from the clustering, resulting in a shift of 0.08σ in S_8. We also test removing mass bin 4, since the stellar mass function cannot correctly reproduce this mass regime, as shown in Fig. 1. For this case, we find similar constraints as when using the full sample (not shown here); this occurs because we actually select the galaxies based on their number density, which mitigates the impact of the different mass functions on the galaxy selection (see Appendix C for more details).

5.2 Extension to all scales of galaxy–galaxy lensing

In Fig. 4 we present cosmological constraints for an extension to our fiducial analysis where we include all scales in the galaxy–galaxy lensing data (green contour). In our fiducial analysis, we remove scales of $\Delta\Sigma$ where $r_p < 1.4\,\text{Mpc}\,h^{-1}$ because the current version of the SHAMe emulator does not include baryonic effects. However, the model works well on small intra-halo scales in the absence of baryons, and in Section 4 we showed that for a simulated analysis, in which the simulated data incorporated the impact of baryonic effects, we were still able to recover the input cosmology when including all scales. It will also be possible to extend the emulator in the future (G. Aricò et al. 2021; M. Zennaro et al. 2025). We therefore explore the consistency of our results with the minimum scale used in the galaxy–galaxy lensing and any potential gains in constraining power.

When we include all scales we find $S_8 = 0.817^{+0.020}_{-0.019}$ and $\Omega_m = 0.279^{+0.017}_{-0.013}$. The S_8 value is 1.26σ higher than our fiducial result and in agreement with *Planck* at the 0.9σ level. We also find a 21 per cent tighter constraint on S_8 and a 29 per cent tighter constraint on Ω_m. This result is consistent with our fiducial result, with the upwards shift in the value of both parameters driven by preference of the small-scale data for the region of high S_8 and Ω_m allowed by the fiducial analysis. An increase in the value of S_8, towards the *Planck* value, is contrary to what might be naively expected when adding small scales without modelling baryonic feedback. In most scenarios, baryonic feedback leads to a suppression of clustering on small scales, which would be interpreted as a lower S_8 if unmodelled (M. Yoon et al. 2019; M. Yoon & M. J. Jee 2021; A. Amon & G. Efstathiou 2022; G. Aricò et al. 2023; C. Preston et al. 2023; C. García-García et al. 2024). This is thus an interesting result in the context of the S_8 tension observed between galaxy surveys and CMB data. Since our data approximately correspond to halo masses of $10^{11.5}$–$10^{13}\,h^{-1}\,M_\odot$ (A. Dvornik et al. 2023), one possible explanation could be that less gas is ejected from low mass haloes.

In Fig. 5 we show our best-fitting clustering and galaxy–galaxy lensing calculated using the maximum posterior values of our all-scale result (green line). We find a good fit to the data with a chi-squared value of 85.5 and a chi-squared per degree of freedom of 1.15, where we simply estimate the degrees of freedom as 84–10. The improvement in the chi-squared value per degree of freedom compared to our fiducial analysis is likely driven by the increase in data points resulting from including all scales. The associated p-value is 0.17, showing that the model is able to describe the small-scale galaxy–galaxy lensing data well.

In Fig. 7 we estimate the impact of not modelling baryonic effects present in the galaxy–galaxy lensing measurements, for both our fiducial (left) and all-scale analysis (right). While it is not possible to fully remove the effect of baryons from our galaxy–galaxy lensing measurements, we can mitigate the impact by subtracting the expected signal predicted by hydrodynamic simulations. We measure this signal by computing the galaxy–galaxy lensing from an SHAMe mock catalogue calibrated to the best-fitting parameters of our all-scale analysis. We then apply the baryonification model from G. Aricò et al. (2021), which displaces the particles of a dark-matter-only simulation to mimic the effect of baryons. The baryonification model reproduces the matter distribution expected for the standard Bahamas simulations (I. G. McCarthy et al. 2017), which are thought to provide the most accurate estimate of baryonic effects in the Universe since they are calibrated using the observed stellar and gas fractions in galaxy clusters. We then measure the difference in the galaxy–galaxy lensing signal between the mock with and without the baryonification implementation, and finally subtract the additional signal from our KiDS-1000 galaxy–galaxy lensing measurements. This allows us to obtain an order-of-magnitude estimate of the impact of baryonic effects.

As expected, in both cases we find that removing baryonic effects increases the value of S_8 to be more consistent with *Planck*. This emphasizes the surprising increase in S_8 found when we move from our fiducial to all-scale analysis (see Fig. 4). For our fiducial analysis, we find a shift of 0.2σ in S_8 when we remove baryonic effects. Without scale cuts, we observe a shift of 0.6σ. We therefore conclude that our fiducial analysis is robust to baryonic effects, and while our all-scale analysis is less conservative, we still find a relatively small impact. These results ultimately depend on the level of feedback in the Universe, and we would expect to find a smaller shift if we were to assume a level of feedback that was smaller than from the Bahamas simulations, or larger, as the one recently predicted by L. Bigwood et al. (2024). While these results are promising, we would like to remind the reader that without a breakthrough on the constraints of baryons in the galaxy–galaxy lensing signal, we need to continue being agnostic to their effect, and therefore we will refer to the results of the fiducial model (i.e. with the limited range of scales in the galaxy–galaxy lensing measurement) as the main result of this work.

5.3 SHAMe parameters

In Fig. 8 we present constraints on the SHAMe parameters (σ, t_{merger}, $f_{k,c+s}$, $f_{k,c-s}$, and β) for our fiducial analysis of GAMA galaxy clustering and KiDS-1000 galaxy–galaxy lensing (blue contour) and

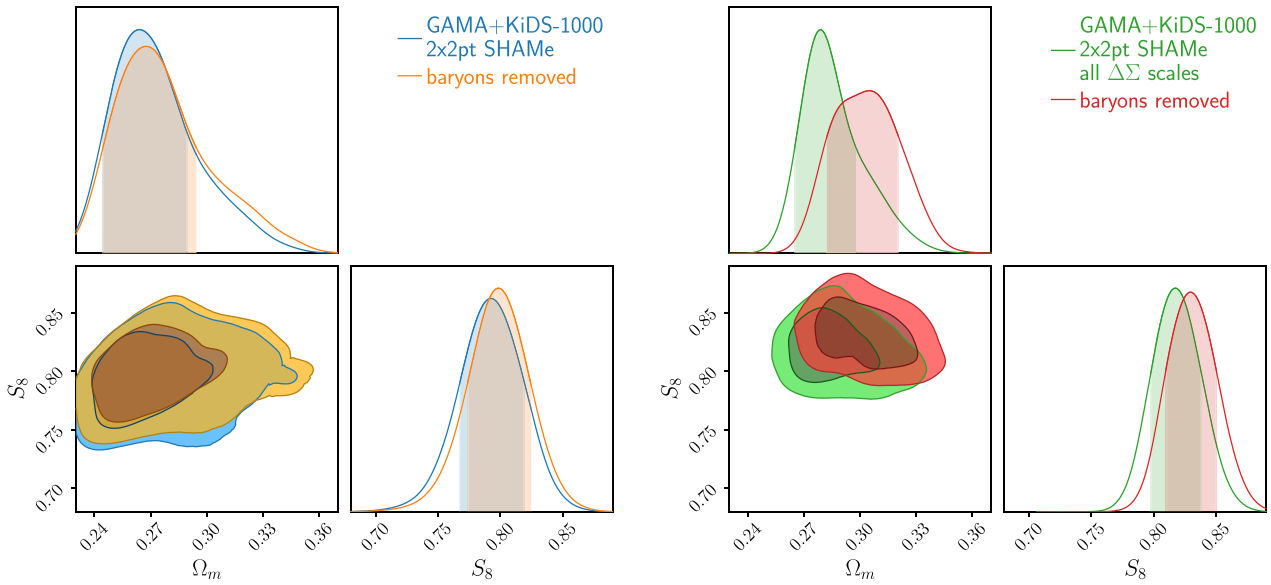

Figure 7. Marginalized posterior constraints on S_8 and Ω_m for GAMA galaxy clustering and KiDS-1000 galaxy–galaxy lensing using SHAMe (left) and the same analysis without scale cuts in the galaxy–galaxy lensing (right). The blue and green contours match those in Fig. 4 and show the analysis with the real data vectors. The orange and red contours show the impact of removing baryons from the data vector, using an estimate from simulations. Our fiducial analysis is robust to baryonic effects, and even our less conservative all-scales analysis is only slightly impacted.

our extended analysis where we include all scales of the galaxy–galaxy lensing (green contour). We are able to constrain all of the SHAMe parameters in both cases, but we find that the inclusion of small-scale $\Delta\Sigma$ data leads to a significant improvement in the constraints on σ $\log M$, $\log t_{\rm merger}$, and β. In turn, this results in the cosmological constraints becoming more precise, highlighting the benefits of including small-scale lensing information when using non-perturbative approaches to describe the clustering of galaxies.

We also find evidence of strong assembly bias for both central and satellite galaxies in the sample. Since $f_{\rm k,c+s}$ and $f_{\rm k,c-s}$ are both positive, there is a positive correlation between large-scale linear bias and the stellar mass or luminosity of a galaxy in the sample (see Section 2.1). If we then populate a mock galaxy catalogue using the best-fitting SHAMe parameters from Fig. 8, we find that this translates to strong assembly bias for both central and satellite galaxies. This implies it is important to model assembly bias in these types of analyses.

In Fig. 8 we additionally show the constraints on the SHAMe parameters for GAMA galaxy clustering alone (orange contour). This illustrates that most of the constraining power on the SHAMe parameters comes from $w_{\rm p}$. $\Delta\Sigma$ alone is only able to constrain σ and β, but when combined with $w_{\rm p}$ in a 2x2pt analysis we are able to constrain all of the SHAMe parameters, as well as S_8 and $\Omega_{\rm m}$. This again illustrates the power of combined analyses of galaxy clustering and galaxy–galaxy lensing.[8]

5.4 Comparison with precursor analysis

In Fig. 4 we also include the $\Omega_{\rm m}$ and S_8 constraints from a precursor analysis of KiDS-1000 galaxy–galaxy lensing, galaxy clustering, and galaxy abundance (2x2pt + SMF; A. Dvornik et al. 2023).[9] The main difference between the two analyses is the modelling of the galaxy–halo connection. A. Dvornik et al. (2023) use an analytical halo model-based description incorporating an effective HOD linked to the conditional stellar mass function. Instead, we use an abundance matching scheme to describe the galaxy–halo connection, extended to include the impact of assembly bias, and with predictions built from the application of this model to N-body simulations (instead of using an analytical approach). A key benefit of SHAMe, in addition to the use of simulations and the inclusion of assembly bias, is its dependence on a smaller number of parameters (five instead of 11). The main disadvantage is that SHAMe requires subhalo information, which is computationally expensive. However, this can be addressed through emulation, and having subhalo information aids in modelling the distribution of satellite galaxies, as it is not necessary to rely on ad hoc parametrizations of the satellite profile. This is particularly useful for galaxy–galaxy lensing (J. Chaves-Montero et al. 2023; S. Contreras et al. 2023a).

The data used in the two analyses are also slightly different. We do not include the lowest two stellar mass bins used in A. Dvornik et al. (2023), resulting in four stellar mass bins instead of six. The lowest two stellar mass bins are currently outside the maximum number density of our SHAMe emulator; however, this limitation will be addressed in future versions. We also use GAMA spectroscopic galaxy clustering instead of KiDS-1000 photometric galaxy clustering (see Section 3 for details). In our fiducial analysis, we do not include small-scale galaxy–galaxy lensing, where $r_{\rm p} < 1.4\,{\rm Mpc}\,h^{-1}$, as we do not explicitly model baryonic effects (see Section 5.2). A. Dvornik et al. (2023) also do not explicitly model baryonic effects but they allow the concentration of both haloes and satellites to vary, which has been shown to provide enough flexibility to account for the impact of baryons (M. Cacciato et al. 2013; M.

[8]The contours in Fig. 8 are the versions without clustering stellar mass bin 3, where $10.5 < \log(M_\star/h^{-2}\,{\rm M}_\odot) \leq 10.7$. See Section 5.1 and Appendix A for details.

[9]The contours look slightly different due to the choice of smoothing scale.

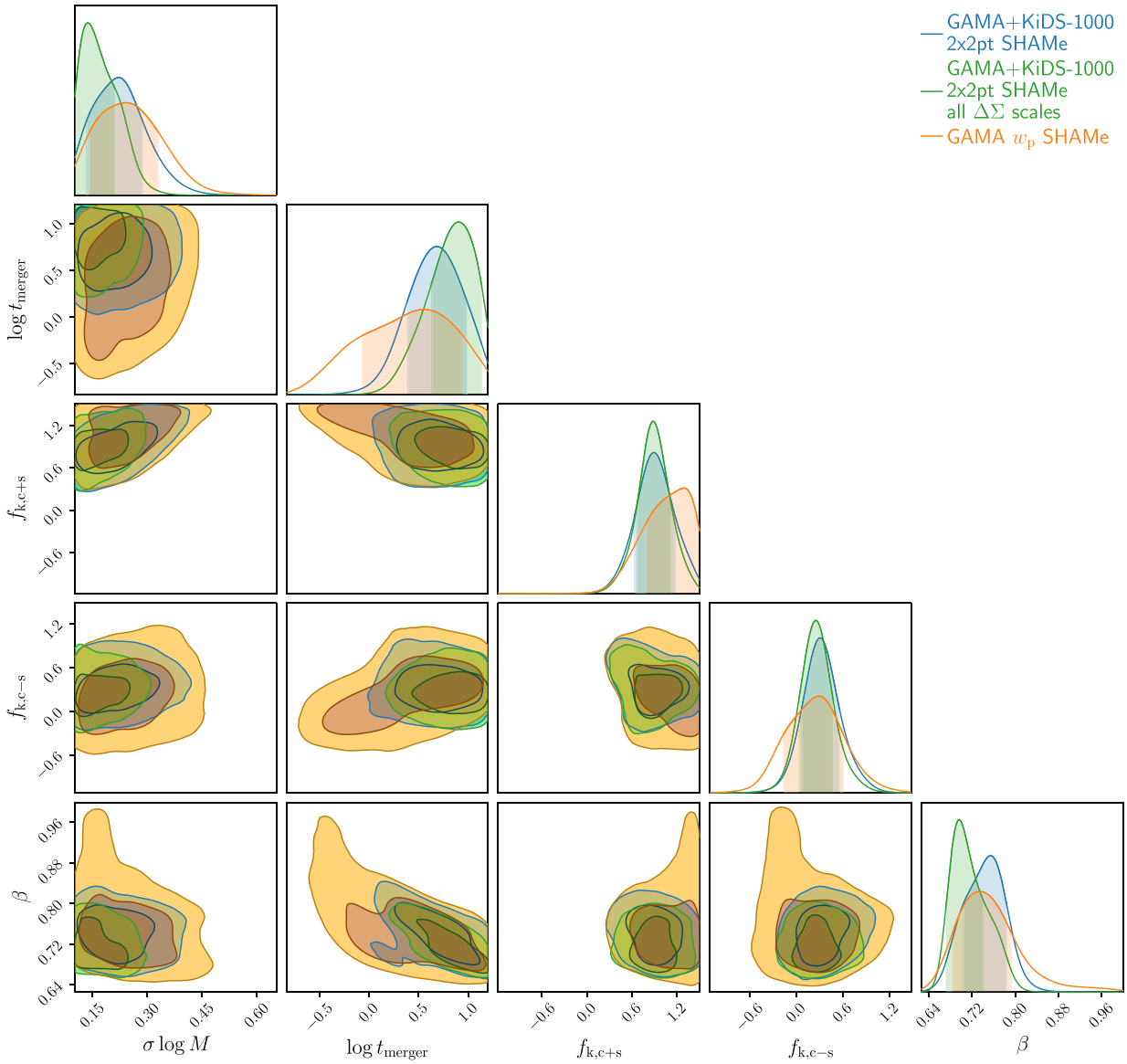

Figure 8. Marginalized posterior constraints on the five SHAMe parameters (σ, $t_{\rm merger}$, $f_{\rm k,c+s}$, $f_{\rm k,c-s}$, and β) for GAMA galaxy clustering and KiDS-1000 galaxy–galaxy lensing using SHAMe (blue), the same analysis without scale cuts in the galaxy–galaxy lensing (green), and for GAMA galaxy clustering alone (orange). We are able to constrain all five SHAMe parameters, as well as the cosmological parameters S_8 and $\Omega_{\rm m}$ (see Fig. 4). The SHAMe parameter constraints predominantly come from the galaxy-clustering, but adding small-scale galaxy–galaxy lensing is also helpful. Note these contours do not include clustering stellar mass bin 3 (see Section 5.1 and Appendix A for details).

Viola et al. 2015; A. Dvornik et al. 2018; E. Uitert et al. 2018; S. N. B. Debackere, J. Schaye & H. Hoekstra 2021; A. Amon et al. 2023). Finally, we include galaxy abundance through the emulator cumulative number density inputs at the stellar mass bin edges (see Section 3.4), instead of jointly modelling the galaxy stellar mass function.

For our fiducial analysis, we find a value of S_8 that is 1.07σ higher than A. Dvornik et al. (2023). This difference increases to 2.65σ when including all scales in $\Delta\Sigma$. We find similar uncertainties on S_8 for our fiducial analysis compared to A. Dvornik et al. (2023), with only a 5 per cent increase in constraining power. This is despite using two fewer stellar mass bins and not including small-scale galaxy–galaxy lensing. For our all-scale analysis, we find our uncertainty on S_8 is improved by 25 per cent compared to A. Dvornik et al. (2023). The consistency between the cosmological constraints found in these two analyses, particularly in the fiducial case, is reassuring, given the vastly different approaches used to model the small-scale clustering of galaxies.

6 CONCLUSION

In this paper we analysed GAMA galaxy clustering and KiDS-1000 galaxy–galaxy lensing using extended SubHalo Abundance Matching (SHAMe) to model the galaxy–halo connection. SHAMe has previously been shown to be capable of simultaneously modelling both galaxy clustering and galaxy–galaxy lensing (S. Contreras et al. 2023a, c), but has not been used to obtain cosmological constraints. In this work we built an emulator to simultaneously model both the

SHAMe and cosmological parameters, and here highlight the most important results:

(i) We validated our analysis by constructing stellar mass-selected samples from the TNG300 hydrodynamic simulation with similar characteristics to those from GAMA and KiDS. We then computed simulated galaxy clustering and galaxy–galaxy lensing data vectors, which we analysed using our SHAMe emulator. We found that we could successfully reproduce both the galaxy clustering and galaxy–galaxy lensing measurements (Fig. 2), as well as correctly recover the input cosmology of the simulation for both our fiducial and all-scale analysis (Fig. 3).

(ii) We jointly analysed four stellar mass bins ($9.95 < \log(M_\star/h^{-2}\,\mathrm{M}_\odot) \leq 11.3$) of GAMA galaxy clustering and KiDS-1000 galaxy–galaxy lensing data using our SHAMe emulator. In our fiducial analysis we found $S_8 = 0.793^{+0.025}_{-0.024}$ and $\Omega_\mathrm{m} = 0.260^{+0.027}_{-0.015}$ (Fig. 4), and were also able to constrain all five SHAMe parameters (Fig. 8). These constraints are consistent with those found by *Planck* within $\mathbf{1.7\sigma}$, and we found a good fit to both the galaxy clustering and galaxy–galaxy lensing data (Fig. 5).

(iii) We extended our fiducial analysis to include scales below $r_\mathrm{p} < 1.4\,\mathrm{Mpc}\,h^{-1}$ in the galaxy–galaxy lensing. We removed these scales in our fiducial analysis to avoid the impact of baryonic effects, which while protecting our results from bias (Fig. 7) limits the constraining power of our approach. When extending our analysis to all scales we found a 21 per cent improvement in our S_8 constraint and a 29 per cent improvement in our Ω_m constraint. We also found a value of S_8, which is 1.26σ higher than our fiducial result, bringing the result into closer agreement with *Planck* ($\sim 1\sigma$) (Fig. 4). Although the statistical evidence of this shift is small, it is interesting to note that such an upwards shift is the opposite of what would be expected in the presence of baryonic feedback, which would normally lead to a suppression in the small-scale clustering of matter (Fig. 7). These results should be interpreted with caution, since our constraints on the impact of baryons on the galaxy–galaxy lensing are still limited, and we therefore cannot make strong statements about these constraints as we can do with the ones where we remove the small scales of the galaxy–galaxy lensing signal, which are the main result of this work. None the less, these results show the power of including smaller scales in the modelling of galaxy clustering observables and the potential of this approach for future analysis.

The results of this paper highlight the potential of joint small-scale galaxy clustering and galaxy–galaxy lensing analyses using SHAMe. We find competitive constraints, which reduce the previously seen tension with *Planck*. The SHAMe model has only five free parameters and, when combined with a scaling technique capable of producing a 1 h^{-1} Gpc dark matter simulation in a matter of minutes (R. E. Angulo & S. D. M. White 2010), we were able to build an emulator using a limited amount of computational resources. These analyses are capable of placing constraints on both cosmological and galaxy formation parameters, including galaxy assembly bias, and provide an exciting prospect for analysing upcoming data from *Euclid* and LSST.

ACKNOWLEDGEMENTS

We thank Marika Asgari for comments on the manuscript, and Jonás Chaves-Montero for writing the code used to compute the galaxy–galaxy lensing from the simulated galaxy catalogues. CM, SC, and REA acknowledge support under the grant number PID2021-128338NB-I00 from the Spanish Ministry of Science. CM and DA acknowledge support from the Beecroft Trust. SC acknowledges the support of the 'Juan de la Cierva Incorporacíon' fellowship (IJC2020-045705-I) and 'Ramón y Cajal' fellowship (RYC2023-043783-I). CG is funded by the MICINN project PID2022-141079NB-C32. IFAE is partially funded by the CERCA program of the Generalitat de Catalunya. AD acknowledges support from an ERC Consolidator Grant (No. 770935).

The authors also acknowledge the computing resources at MareNostrum and the technical support provided by Barcelona Supercomputing Center (RES-AECT-2024-2-0022). Technical and human support provided by DIPC Supercomputing Center is gratefully acknowledged.

GAMA is a joint European-Australasian project based around a spectroscopic campaign using the Anglo-Australian Telescope. The GAMA input catalogue is based on data taken from the Sloan Digital Sky Survey and the UKIRT Infrared Deep Sky Survey. Complementary imaging of the GAMA regions is being obtained by a number of independent survey programmes including GALEX MIS, VST KiDS, VISTA VIKING, WISE, Herschel-ATLAS, GMRT, and ASKAP providing UV to radio coverage. GAMA is funded by the STFC (UK), the ARC (Australia), the AAO, and the participating institutions. The GAMA website is https://www.gama-survey.org/.

Based on observations made with ESO Telescopes at the La Silla Paranal Observatory under programme IDs 177.A-3016, 177.A-3017, 177.A-3018, and 179.A-2004, and on data products produced by the KiDS consortium. The KiDS production team acknowledges support from Deutsche Forschungsgemeinschaft, ERC, NOVA, and NWO-M grants; Target; the University of Padova, and the University Federico II (Naples).

DATA AVAILABILITY

The data underlying this article will be shared on reasonable request to the corresponding authors.

REFERENCES

Abadi M. et al., 2015, TensorFlow: Large-Scale Machine Learning on Heterogeneous Systems
Abbott T. M. C. et al., 2022, Phys. Rev. D, 105, 023520
Amon A. et al., 2023, MNRAS, 518, 477
Amon A., Efstathiou G., 2022, MNRAS, 516, 5355
Angulo R. E., Pontzen A., 2016, MNRAS, 462, L1
Angulo R. E., White S. D. M., 2010, MNRAS, 405, 143
Angulo R. E., Zennaro M., Contreras S., Aricò G., Pellejero-Ibañez M., Stücker J., 2021, MNRAS, 507, 5869
Aricò G., Angulo R. E., Contreras S., Ondaro-Mallea L., Pellejero-Ibañez M., Zennaro M., 2021, MNRAS, 506, 4070
Aricò G., Angulo R. E., Zennaro M., Contreras S., Chen A., Hernández-Monteagudo C., 2023, A&A, 678, A109
Arnouts S., Cristiani S., Moscardini L., Matarrese S., Lucchin F., Fontana A., Giallongo E., 1999, MNRAS, 310, 540
Baldry I. K. et al., 2012, MNRAS, 421, 621
Beutler F. et al., 2017, MNRAS, 466, 2242
Bigwood L. et al., 2024, MNRAS, 534, 655
Bilicki M., et al., 2021, A&A, 653, A82
Cacciato M., Bosch F. C. v. d., More S., Li R., Mo H. J., Yang X., 2009, MNRAS, 394, 929
Cacciato M., van den Bosch F. C., More S., Mo H., Yang X., 2013, MNRAS, 430, 767
Chaves-Montero J., Angulo R. E., Contreras S., 2023, MNRAS, 521, 937
Chaves-Montero J., Angulo R. E., Schaye J., Schaller M., Crain R. A., Furlong M., Theuns T., 2016, MNRAS, 460, 3100
Contreras S. et al., 2023b, MNRAS, 524, 2489

Contreras S., Angulo R. E., Chaves-Montero J., Kugel R., Schaller M., Schaye J., 2024, A&A, 690, A311
Contreras S., Angulo R. E., Chaves-Montero J., White S. D. M., Aricò G., 2023a, MNRAS, 520, 489
Contreras S., Angulo R. E., Zennaro M., 2021a, MNRAS, 504, 5205
Contreras S., Angulo R. E., Zennaro M., 2021b, MNRAS, 504, 5205
Contreras S., Angulo R. E., Zennaro M., 2021c, MNRAS, 508, 175
Contreras S., Angulo R. E., Zennaro M., Aricò G., Pellejero-Ibañez M., 2020, MNRAS, 499, 4905
Contreras S., Chaves-Montero J., Angulo R. E., 2023c, MNRAS, 525, 3149
Croton D. J., Gao L., White S. D. M., 2007, MNRAS, 374, 1303
d'Amico G., Gleyzes J., Kokron N., Markovic K., Senatore L., Zhang P., Beutler F., Gil-Marín H., 2020, J. Cosmol. Astropart. Phys., 2020, 005
Dalal N., White M., Bond J. R., Shirokov A., 2008, ApJ, 687, 12
Debackere S. N. B., Schaye J., Hoekstra H., 2021, MNRAS, 505, 593
Driver S. P. et al., 2011, MNRAS, 413, 971
Driver S. P. et al., 2022a, MNRAS, 513, 439
Driver S. P. et al., 2022b, MNRAS, 513, 439
Dvornik A. et al., 2018, MNRAS, 479, 1240
Dvornik A., et al., 2023, A&A, 675, A189
Edge A., Sutherland W., Kuijken K., Driver S., McMahon R., Eales S., Emerson J. P., 2013, The Messenger, 154, 32
Euclid Collaboration, 2025, A&A, 697, A1
Farrow D. J. et al., 2015, MNRAS, 454, 2120
Gao L., Springel V., White S. D. M., 2005, MNRAS, 363, L66
García-García C., Zennaro M., Aricò G., Alonso D., Angulo R. E., 2024, J. Cosmol. Astropart. Phys., 2024, 024
Georgiou C., Chisari N. E., Bilicki M., La Barbera F., Napolitano N. R., Roy N., Tortora C., 2025, A&A, 699, A252
Giblin B. et al., 2021, A&A, 645, A105
Guo Q., White S., 2014, MNRAS, 437, 3228
Hearin A. P., Zentner A. R., van den Bosch F. C., Campbell D., Tollerud E., 2016, MNRAS, 460, 2552
Heymans C., et al., 2021, A&A, 646, A140
Hildebrandt H. et al., 2021, A&A, 647, A124
Ilbert O. et al., 2006, A&A, 457, 841
Ivanov M. M., Simonović M., Zaldarriaga M., 2020, J. Cosmol. Astropart. Phys., 2020, 042
Ivezić Ž. et al., 2019, ApJ, 873, 111
Jarvis M., Bernstein G., Jain B., 2004, MNRAS, 352, 338
Johnston H. et al., 2019, A&A, 624, A30
Krause E. et al., 2021, preprint (arXiv:2105.13548)
Kuijken K. et al., 2019, A&A, 625, A2
Lange J. U., 2023, MNRAS, 525, 3181
Lange J. U., van den Bosch F. C., Zentner A. R., Wang K., Hearin A. P., Guo H., 2019, MNRAS, 490, 1870
Mahony C. et al., 2022, MNRAS, 515, 2612
McCarthy I. G., Schaye J., Bird S., Le Brun A. M. C., 2017, MNRAS, 465, 2936
Mead A. J., Brieden S., Tröster T., Heymans C., 2021, MNRAS, 502, 1401
Mead A. J., Verde L., 2021, MNRAS, 503, 3095
Miyatake H. et al., 2022, Phys. Rev. D, 106, 083519
Miyatake H. et al., 2023, Phys. Rev. D, 108, 123517
More S., van den Bosch F. C., Cacciato M., More A., Mo H., Yang X., 2013, MNRAS, 430, 747
Nelson D., et al., 2019, Comput. Astrophys. Cosmol., 6, 2
Nicola A. et al., 2024, J. Cosmol. Astropart. Phys., 2024, 015
Nishimichi T. et al., 2019, ApJ, 884, 29
Paranjape A., Hahn O., Sheth R. K., 2018, MNRAS, 476, 3631
Planck Collaboration VI, 2020, A&A, 641, A6
Preston C., Amon A., Efstathiou G., 2023, MNRAS, 525, 5554
Sinha M., Garrison L. H., 2020, MNRAS, 491, 3022
Smith R. E. et al., 2003, MNRAS, 341, 1311
Stölzner B. et al., 2025, A&A, 702, A169
Takahashi R., Sato M., Nishimichi T., Taruya A., Oguri M., 2012, ApJ, 761, 152
Taylor E. N. et al., 2011, MNRAS, 418, 1587
van den Bosch F. C., More S., Cacciato M., Mo H., Yang X., 2013, MNRAS, 430, 725
van Uitert E. et al., 2018, MNRAS, 476, 4662
Viola M. et al., 2015, MNRAS, 452, 3529
Wang L. et al., 2013, MNRAS, 431, 648
Wechsler R. H., Zentner A. R., Bullock J. S., Kravtsov A. V., Allgood B., 2006, ApJ, 652, 71
Wright A. H. et al., 2024, A&A, 686, A170
Wright A. H. et al., 2025, A&A, 703, A158
Yang X., Mo H. J., Bosch F. C. v. d., 2008, ApJ, 676, 248
Yoon M., Jee M. J., 2021, ApJ, 908, 13
Yoon M., Jee M. J., Tyson J. A., Schmidt S., Wittman D., Choi A., 2019, ApJ, 870, 111
Zennaro M. et al., 2025, MNRAS, 544, 3512

APPENDIX A: INTERNAL INCONSISTENCY IN CLUSTERING DATA

When analysing GAMA clustering alone to check the internal consistency of our data we found a strong constraint on S_8, which is not expected from clustering data alone and was inconsistent with our fiducial result. This constraint is shown in Fig. A1 (blue contour). To determine where this spurious constraint was coming from we first analysed the clustering data removing each of the four stellar mass bins in turn. We found that if we removed bin 3, where $10.5 < \log(M_\star/h^{-2}\,\mathrm{M}_\odot) \leq 10.7$, the strong constraint on S_8 disappeared (orange contour). Next, we varied the scales included in bin 3 and found that if we removed large scales, where $r_{\rm max} > 1.5\ h^{-1}$ Mpc, the strong constraint on S_8 also disappeared (green contour). This led us to conclude that there is likely an uncontrolled systematic effect impacting the large scales of clustering bin 3. When we removed stellar mass bin 3 from the clustering in our fiducial joint analysis of

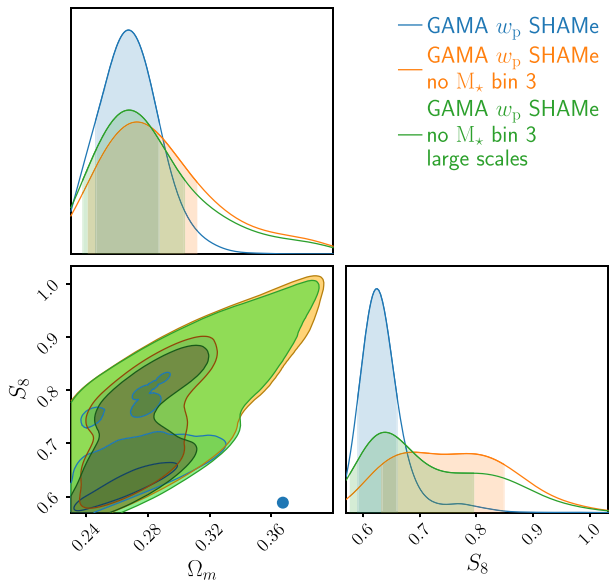

Figure A1. Marginalized posterior constraints on S_8 and $\Omega_{\rm m}$ for GAMA galaxy clustering alone using SHAMe with stellar mass bin 3 (blue), without stellar mass bin 3 (orange), and without the large scales of stellar mass bin 3 (green). Stellar mass bin 3 includes $10.5 < \log(M_\star/h^{-2}\,\mathrm{M}_\odot) \leq 10.7$, and we define large scales as $r_{\rm max} = 1.5\ h^{-1}$ Mpc. Including bin 3 we find a strong constraint on S_8, which is inconsistent with our fiducial combined analysis. When we remove bin 3, or even just the large scales of bin 3, this internal inconsistency disappears.

GAMA galaxy clustering and KiDS-1000 galaxy–galaxy lensing we found very little impact on our results (see Fig. 6).

APPENDIX B: ANALYTIC PREDICTION OF THE CORRELATION FUNCTION OF GALAXIES SELECTED IN A STELLAR MASS BIN

We derived equation (7),

$$w_{\rm p}(M_{\star 1} < M_\star < M_{\star 2}) \simeq w_{\rm p1}\left(\frac{n_1}{n_1-n_2}\right)^2 + w_{\rm p2}\left(\frac{n_2}{n_1-n_2}\right)^2 - 2\sqrt{w_{\rm p1}w_{\rm p2}}\left(\frac{n_1 n_2}{(n_1-n_2)^2}\right), \tag{B1}$$

by assuming that the galaxies of the sample are selected using a number density cut of n_1, but not n_2. The amplitude of the clustering signal scales as n_2, and the number of objects in the new sample is $(n_1 - n_2)$. Assuming the correlation function goes as the δ, we can define the amplitude of the bin (from the galaxies that are in sample 1 but not sample 2) as

$$\delta_{\rm bin}(\mathbf{x}) = \frac{n_1\,\delta_1(\mathbf{x}) - n_2\,\delta_2(\mathbf{x})}{n_1 - n_2}. \tag{B2}$$

And since the correlation function between a sample 'a' and a sample 'b' goes as $\langle\delta_a\delta_b\rangle$,

$$w_{p,\rm bin}(r_p) = \left(\frac{n_1}{n_1-n_2}\right)^2 w_{p,11}(r_p) + \left(\frac{n_2}{n_1-n_2}\right)^2 w_{p,22}(r_p) - 2\,\frac{n_1 n_2}{(n_1-n_2)^2}\,w_{p,12}(r_p). \tag{B3}$$

From these terms, the only one we do not have from our emulator is the last term, but we can approximate it to

$$w_{p,12}(r_p) \approx \alpha\,\sqrt{w_{p,11}(r_p)\,w_{p,22}(r_p)}, \qquad \alpha \simeq 1, \tag{B4}$$

with α affected by the (non)correlation of the samples and the differences in bias. For the bins in mass we used in this work, we have a difference of ~ 1 per cent. We perform a similar analysis for equation (8).

APPENDIX C: COSMOLOGICAL CONSTRAINTS EXCLUDING STELLAR MASS BIN 4

As mentioned in Section 5.1, the galaxy selection is performed using cuts in number density rather than stellar mass. This approach mitigates the impact of discrepancies in the stellar mass function, which become substantial at the high–mass end, on the clustering measurements. In Fig. C1 we examine the cosmological constraints obtained after removing this bin and find that they remain in good agreement with those derived from the main sample. Consequently, we conclude that our implementation adequately accounts for the differences in the stellar mass function for this subsample.

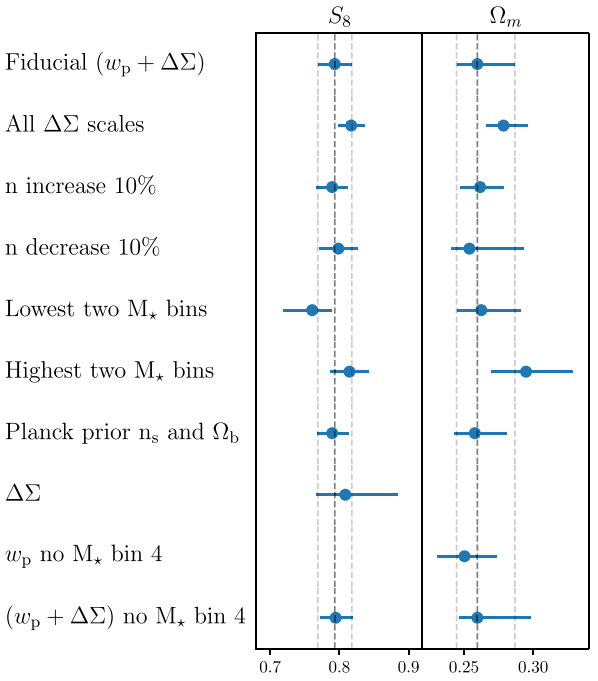

Figure C1. Similar to Fig. 6, but excluding the stellar mass bin 4 instead of the stellar mass bin 3.

This paper has been typeset from a TEX/LATEX file prepared by the author.